Long-chain GM1 gangliosides alter transmembrane domain registration through interdigitation

Moutusi Manna,[a,♯] Matti Javanainen,[a,b,♯] Hector Martinez-Seara Monne,[a,c] Hans-Joachim Gabius,[d] Tomasz Rog,[a,b] and Ilpo Vattulainen[a,b,e,*]

[a] Department of Physics, Tampere University of Technology, P. O. Box 692, FI- 33101 Tampere, Finland

[b] Department of Physics, POB 64, FI-00014 University of Helsinki, Finland

[c] Institute of Organic Chemistry and Biochemistry, Academy of Sciences of the Czech Republic, CZ-16610 Prague, Prague, Czech Republic

[d] Institute of Physiological Chemistry, Faculty of Veterinary Medicine, Ludwig Maximilian University, D-80539 Munchen, Germany

[e] MEMPHYS-Center for Biomembrane Physics, University of Southern Denmark, Odense, Denmark

[♯] These two authors contributed equally to the article.

*Correspondence to be sent to: Ilpo.Vattulainen@helsinki.fi

Abstract

Extracellular and cytosolic leaflets in cellular membranes are distinctly different in lipid composition, yet they contribute together to signaling across the membranes. Here we consider a mechanism based on long-chain gangliosides for coupling the extracellular and cytosolic membrane leaflets together. Based on atomistic molecular dynamics simulations, we find that long-chain GM1 in the extracellular leaflet exhibits a strong tendency to protrude into the opposing bilayer leaflet. This interdigitation modulates the order in the cytosolic monolayer and thereby strengthens the interaction and coupling across a membrane. Coarse-grained simulations probing longer time scales in large membrane systems indicate that GM1 in the extracellular leaflet modulates the phase behavior in the cytosolic monolayer. While short-chain GM1 maintains phase-symmetric bilayers with a strong membrane registration effect, the situation is altered with long-chain GM1. Here, the significant interdigitation induced by long-chain GM1 modulates the behavior in the cytosolic GM1-free leaflet, weakening and slowing down the membrane registration process. The observed physical interaction mechanism provides a possible means to mediate or foster transmembrane communication associated with signal transduction.

Key words:

Glycosphingolipid, cholesterol, membrane domain, membrane registry, molecular dynamics, computer simulations

Introduction

Cells invest substantial resources to synthesize a broad range of membrane lipids and to maintain their asymmetric inhomogeneous distributions in biological membranes [1, 2]. In addition to roles in maintaining membrane stability and fluidity, awareness is growing that the headgroups of glycosphingolipids (GSLs) are of particular relevance for recognition processes, especially by tissue lectins [3-5]. Notably the presence of glycolipids and the mode of presentation are of critical significance to serve as functional counterreceptors [6]. In this respect, organization of lipids as in-plane membrane domains has been studied for decades [7-9], yet an understanding of domain structure and composition, and the biological function of domains overall, is still quite incomplete. The concept of lipid rafts [10-12] (functional nanoscale domains rich in cholesterol, saturated phospholipids, and bioactive lipids such as gangliosides) as well as different interpretations of research data [13] concur with the existence of functional membrane units comprised of proteins and lipids, where lipid-protein interactions modulate several aspects of protein activity [14]. This suggests that membrane-associated proteins can reorganize their membrane environment to be rich in lipids that modulate protein features dynamically. In comparison, under protein-free conditions the existence of membrane domains with different lipid compositions and physical properties is well established [15]. Studies on model membranes have unambiguously shown macroscopic phase separation into cholesterol-rich liquid-ordered (L_o) and cholesterol-poor liquid-disordered (L_d) domains in a manner [16, 17], where the phase separation in the bilayer plane arises from lipid-dependent liquid-liquid immiscibility.

Due to their already noted asymmetry, the two leaflets of biological membranes are also different in composition [1, 2]. The lipid mixture that is typical for the extracellular leaflet of eukaryotic plasma membranes contains sphingolipids with a high percentage of cholesterol. It tends to phase separate when reconstituted in model membranes. In contrast, such phase separation does not take place for the lipid mixture that represents the cytoplasmic leaflet enriched in, e.g., unsaturated lipids [18, 19].

The distinctly different transmembrane compositions of biological membranes can lead to phase asymmetry or antiregistration, meaning that L_o and L_d domains overlap each other in the two opposite leaflets [20,21]. Meanwhile, a domain in one leaflet can induce formation of a similar domain also in the opposite leaflet (i.e., both being in the L_o or L_d phase), leading to phase symmetry or registration [20-22]. Several mechanisms for protein-independent domain induction between membrane leaflets have been proposed, including

interfacial energy minimization [23], electrostatic coupling [20], lipid and cholesterol flip-flop [20, 24], composition-curvature coupling [25, 26], and dynamic chain interdigitation [20, 27, 28]. However, despite considerable research efforts, there is no consensus on whether biological membranes are phase symmetric or asymmetric. Furthermore, the exact mechanism of induced domain formation remains undetermined.

There is evidence in favor of both bilayer registration and antiregistration [18, 20, 23, 29] but the overall understanding of their causes is still unclear. This partly stems from difficulties to carry out robust and unambiguously interpretable experiments on domains in biological membranes, where, for instance, one applies methods such as detergent extraction that is unable to characterize the phases in individual bilayer leaflets. On the other hand, experiments on asymmetric model membranes are carried out under non-equilibrium conditions, right after the formation of an asymmetric membrane, since lipid flip-flops quite rapidly lead to transbilayer symmetry. Although these studies have significantly enhanced our current understanding of this topic, the interpretation of experimental data is admittedly not straightforward.

Theoretical and simulation studies provide another means to explore the coupling between membrane domains in different leaflets and to elucidate the physical principles that lead to domain registration and/or antiregistration [20, 26, 30-33]. These studies have suggested that the coupling of phase behavior between the leaflets is highly sensitive to lipid composition, yet it is not well understood why certain lipid mixtures induce domain registration whereas others do not.

Based on the concept of the sugar code that ascribes informational contents to glycans presented by scaffolds (sphingolipids, proteins) [34-36], giving special attention to GSLs is warranted. GSLs are integral components of ordered lipid domains [37, 38], and their carbohydrate headgroup is linked to a ceramide moiety, exclusively sorted to the extracellular leaflet of plasma membranes, where they can engage in biorecognition [39, 40]. We here focus on ganglioside GM1, a so-called true factotum of nature [41], because it is a counterreceptor for adhesion/growth-regulatory galectins, hereby involved for example in effector/regulatory T cell communication, lectin endogytosis, neuritogenesis, and neuroblastoma growth arrest [42-47]. To efficiently do so, positional aspects (density and presentation) appear crucial [48]. Notably, the interaction with the human bioeffector has also been analyzed in model membranes without proteins [49]. Looking at the structure of GSLs, a source of variability concerns the length of the acyl chain. While the majority of phospholipids have acyl chains with 16 to 18 carbons, GSLs can typically have considerably

longer chains that consist of 24 carbons or more [50-52], allowing GSLs to pack tightly into ordered membrane domains. The long hydrocarbon chains may promote greater exposure of the carbohydrate headgroup and therefore enhance ligand binding of GSLs [51]. In fact, the routing signal for apical and axonal transport of glycoproteins by galectin-4, i.e. the sulfatide headgroup, is presented preferentially by ceramide with long (C24)-chain fatty acids [52-54]. As a further consequence, a long tail can extend into the opposite bilayer leaflet through interdigitation and thereby provide a potential means for signal transduction [50]. Given that contribution by both modes of placement of the long acyl chain can be of physiological relevance, consideration of the effect of GSL chain length on membrane registration is of interest.

To address this issue, we carried out a series of atomistic and coarse-grained molecular dynamics (MD) simulations on many-component membranes with GM1 to unravel how its acyl chain length (ranging from 16 to 30 carbons) contributes to membrane registration. We found that long-chain GM1 interdigitates to a substantial degree to the opposite membrane leaflet and alters its phase behavior.

Methods

Atomistic simulations of symmetric bilayers

We used all-atom MD simulations to consider eight types of model membranes that were composed of 1-palmitoyl-2-oleoyl-*sn*-glycero-3-phosphocholine (POPC) (202 molecules), GM1 (14 molecules), and cholesterol (Chol) (72 molecules). These eight systems were also simulated in the absence of cholesterol. The molar concentrations of GM1 (POPC) were therefore 4.9 (70.1) and 6.5 (93.5) mol% in systems with and without cholesterol, respectively. Cholesterol concentration was 25 mol% in the three-component system (Table 1). The transmembrane lipid distributions were in all systems symmetric. The factor that differentiates the eight types of bilayers is the length of the fatty acid acyl chain of GM1: it ranged from palmitic acid (16:0, referred to as $GM1_{16}$) to melissic acid (30:0, referred to as $GM1_{30}$). Given the abundance of both POPC and cholesterol, the POPC/cholesterol/GM1 mixture provides an appropriate basis to consider the effects of GM1 in a system, whose phase behavior has been suggested to be rich, especially when it is extended with other lipid components (see, e.g., [55]). Figure 1 shows the chemical structure of all lipid molecules

involved in this study. Bilayers were extensively hydrated with 13785 water molecules, and 14 Na^+ counterions were added to neutralize the excess charge of GM1.

Lipid molecules were described by the all-atom OPLS force field [56] with recent extensions for carbohydrates [57] and lipids [58-61]. Water was described by the TIP3P model [62] that is compatible with the OPLS-AA force field. Prior to MD simulations the systems were energy-minimized using the steepest-descend algorithm. For each of the 16 systems, an MD simulation of 400 ns was conducted using the GROMACS 4.6.6 software package [63]. The first 100 ns period of the trajectories was considered as equilibration and the last 300 ns of the trajectories were used for analyses.

Simulations were performed in the isobaric-isothermal (NpT) ensemble (310 K and 1 bar). The temperature of the system was maintained by the velocity-rescaling (v-rescale) thermostat with a time constant of 0.1 ps [64]. The temperatures of the solute and the solvent were controlled independently. The pressure of the system was maintained semiisotropically by the Parrinello–Rahman barostat with a 1 ps time constant [65]. The time step for integration of equations of motion was set to 2 fs. Periodic boundary conditions were imposed in all three dimensions. For the long-range electrostatic interactions, the particle-mesh Ewald (PME) method was used [66]. Lennard–Jones interactions were cutoff at a distance of 1.0 nm. The linear constraint solver (LINCS) algorithm was used to preserve covalent bond lengths [67].

Coarse-grained simulations of asymmetric bilayers

To study the effect of acyl chain length of GM1 on membrane phase behavior, we employed the coarse-grained Martini model [68-70]. A bilayer consisting of 1348 lipids (674 in each leaflet) was first constructed as a random arrangement of 30 mol% palmitoylsphingomyelin (PSM), 40 mol% dilinoleylphosphatidylcholine (DLiPC), and 30 mol% cholesterol (Figure 1). This system was then used for preparing four systems with varying concentration and acyl chain length of GM1 (Table 1). First, either 1.5 or 6.0 mol% of GM1 was inserted into the upper leaflet by randomly replacing existing lipids from this leaflet with GM1 in a manner where the 30:40:30 ratio between PSM, DLiPC, and cholesterol, respectively, was maintained. Second, the fatty acid attached to these GM1 molecules was chosen to be either five (referred to as $GM1_{short}$) or eight beads (referred to as $GM1_{extended}$) long (Figure 1). The "short" and "extended" cases correspond to GM1 molecules with an acyl chain of ~18 and ~30 carbons, respectively. The ternary DLiPC/PSM/cholesterol system chosen for coarse-grained simulations is largely the standard system employed in phase separation studies

using the Martini approach (see, e.g., refs. [71,72]). The systems were hydrated with 18110 water beads. About 150 mM of NaCl was added to the system together with counterions to compensate for the charge of GM1s.

The four GM1-containing bilayers were simulated for 10 μs each, using a time step of 5 fs. We performed 10 repeats for each bilayer (4 x 10 x 10 μs) (Table 1). A GM1-free control system (as a symmetric bilayer) was simulated for 10 μs with a time step of 25 fs (Table 1). For the GM1-free control system, we performed 8 repeats. The temperature of the lipids and the solvent were separately maintained at 300 K using the velocity-rescaling thermostat with a time constant of 1 ps [64]. Pressure was coupled semiisotropically to the Parrinello–Rahman barostat [65]. A reference pressure of 1 bar was employed, and the coupling time was set to 12 ps. The Verlet cutoff scheme was employed for nonbonded interactions. Electrostatic interactions were handled with the reaction field method with a cut-off of 1.1 nm and the relative permittivity of 15. The potential shift modifier was employed for the Lennard–Jones interactions and a cut-off of 1.1 nm was used. Periodic boundary conditions were employed in all three dimensions. All coarse-grained simulations were run with GROMACS 5.0.x [73].

Analyses

Area per lipid was calculated by dividing the time-averaged total area of the simulation box (in the bilayer plane) by the number of lipids in a single leaflet. Bilayer thickness was computed from the distance between average positions of phosphate atoms in the two bilayer leaflets. The deuterium order parameter S_{CD} describing the conformational order along lipid acyl chains is defined for each carbon in the chain as in [74]:

$$S_{\mathrm{CD},i} = \langle \frac{3}{2} \cos^2 \theta_i - \frac{1}{2} \rangle,$$

where θ_i is the angle between a C–D bond (C–H in simulations) for carbon number i and the bilayer normal. The angular brackets denote averaging over time and lipids of the same type.

To characterize the conformation of GM1's pentasaccharide, we analyzed the orientation of the GM1 headgroup in terms of three vectors depicted in Figure S1. The first vector was named as *Wrist* based on its location in the GM1 headgroup, describing the orientation of the first sugar (Glc) that is O-glycosidically connected to ceramide. The two

other vectors (*Thumb* and *Forefinger*) characterize the orientations of the two outermost branches in the GM1 head group (Figure S1) that are the contact sites for human and bacterial lectins [75]. The angles between these vectors and the bilayer normal provide an overall picture of the head group conformation.

Interdigitation between the two membrane leaflets is characterized by the overlap parameter $q_{oi}(z)$ as [76]

$$q_{oi}(z) = 4\frac{q_i(z)q_o(z)}{[q_i(z)+q_o(z)]^2},$$

where z is the coordinate in the membrane normal direction, and $q_i(z)$ and $q_o(z)$ are the number densities of atoms belonging to the inner and outer leaflets, respectively, calculated from a trajectory centered at the middle of a bilayer center. When the overlap parameter is integrated over the membrane along the bilayer normal direction (over the simulation box from zero to *d*), one finds the length scale

$$\lambda = \int_o^d q_{oi}(z)\mathrm{d}z\,,$$

where λ describes in a suggestive fashion the length scale over which the two monolayers are interdigitated. Here, one has to keep in mind that λ does not describe the extent of interdigitation of individual lipid chains. Rather, it provides a measure for the average interdigitation between the two leaflets.

In CG simulations of the many-component membranes, we quantified the extent of in-plane phase separation by the contact fraction between saturated (PSM) and unsaturated (DLiPC) lipids using the approach of Domanski et al. [77],

$$f_{\mathrm{mix}} = \frac{c_{\mathrm{DLiPC-PSM}}}{c_{\mathrm{DLiPC\text{-}PSM}} + c_{\mathrm{DLiPC\text{-}DLiPC}}},$$

where $c_{\mathrm{DLiPC-PSM}}$ denotes contacts between the phosphate (PO4) beads of DLiPC and PSM molecules. Here, a cut-off distance of 1.1 nm was employed for the determination of contacts. The contact fraction f_{mix} was computed only within the GM1-free leaflet of the asymmetric CG membrane. In a randomly distributed leaflet with no phase separation, f_{mix} is

large (e.g., about 0.41 in the CG system with 6 mol% GM1), but decreases the more the more the system phase separates.

The rate of phase separation was quantified by fitting the time evolution of the contact fractions (f_{mix}) with an exponentially decaying function

$$f_{\mathrm{mix}}(t) = Ae^{-t/\tau} + b \ ,$$

where A and b are constants related to the initial and final levels of separation, t is the simulation time, and τ is a decay constant associated with the phase separation process.

In CG model systems, where phase separation into L_o and L_d domains was observed, we analyzed the transbilayer domain registration of regions with a similar degree of order, *i.e.* the membrane registry effect. To this end, for every analyzed frame, the saturated (PSM) and unsaturated (DLiPC) lipids were binned onto a 2D grid based on the position of the phosphate bead (PO4). The cell area was set to 1 nm^2 and the binning was performed every 10 ns. Then, we checked whether the corresponding cells in the 2D grids of the two leaflets were mostly occupied by the same lipid type (saturated vs. unsaturated). If this condition was satisfied, transbilayer domain registration for this cell was registered. The number of cells with observed coupling was then counted for each studied frame, and the data were normalized so that the value of one stands for perfect registry, where an L_o domain of one leaflet faces an L_o domain of the opposing leaflet, and similarly an L_d domain faces an L_d domain of the opposing leaflet. Similarly, the value of zero stands for perfect antiregistration, where an L_o domain in one leaflet faces an L_d domain of the opposing leaflet and vice-versa. Intermediate values describe the fraction of the system that is in registry.

In consideration of lateral diffusion, where the aim was to determine whether GM1 interdigitation affects the fluidity in the opposing leaflet (see the results below), the mean-squared displacement (MSD) of lipids was calculated from the first 2 μs, i.e., from the region in time where phase separation takes place. The fits to linear behavior in time were performed to the MSD data between 20–200 ns lag times.

Results

Long acyl chains of GM1 induce interleaflet coupling and ordering that span the whole membrane

Snapshots of atomistic simulations (Figure 2) clearly show the tendency of long acyl chains of GM1 to extend deep into the opposing bilayer leaflet. There is a significant reorganization of hydrocarbon chains at the midplane of the bilayer as demonstrated by the density profiles of the long acyl chains depicting a peak in the bilayer center, in contrast to a dip observed with short-tail GM1 (see Figure S2 in Supplementary Information).

To quantify interdigitation in more detail, Figure S3 shows the partial densities of the terminal carbon atoms of the acyl and sphingosine tails of $GM1_{16}$ and $GM1_{30}$, as well as of the terminal carbon of the POPC *sn*-2 chain. The results for $GM1_{30}$ are quite revealing. The terminal carbon of the GM1 acyl chain protrudes about 2 nm into the opposite layer. This means that $GM1_{30}$ penetrates *through* the membrane to the head group region in the opposing membrane leaflet. The distribution of $GM1_{30}$ also has two maxima: the first maximum is located in the middle of the bilayer, characterizing acyl chains that lie along the membrane plane in the free volume cavity, and the second maximum resides deep in the opposite leaflet about 1.5 nm from the bilayer center. Cholesterol strengthens interdigitation, but the interdigitation is exceptionally pronounced without cholesterol, too. The two quite different orientations are also evident from the simulation snapshots in Figure 2. Meanwhile, the terminal carbons of $GM1_{16}$, the GM1 sphingosine chains, and the POPC *sn*-2 chain behave regularly.

The threshold length of GM1 to observe the double-peak structure in the terminal carbon distribution is about 24 (Figure 3). For shorter acyl chains, calculations for GM1 result in a single peak around the membrane center. For chain lengths of 24 and longer, the double-peak structure arises and becomes more and more prominent for increasing acyl chain length. Cholesterol increases the effect.

Figure 4 highlights the above-discussed findings in terms of λ, which characterizes the length scale over which the two leaflets come into contact to a significant degree. The interdigitation becomes stronger for increasing GM1 acyl chain length. As to the role of cholesterol, $GM1_{30}$ in the absence of cholesterol results in the same value for λ as $GM1_{16}$ in the presence of cholesterol.

Interdigitation of long acyl chains of GM1 has a quite dramatic effect on the acyl chain conformational order described by S_{CD} (Figure 5). When the length of the acyl chains rises above ~24, the order parameter profile first levels off and then starts to increase again, reflecting how the terminal region of the GM1 acyl chain aligns with the hydrocarbon chains in the opposing leaflet. The effect is exceptionally strong with cholesterol. Similar behavior

with long acyl chains was recently observed for sphingomyelin in atomistic MD simulations [27], and with long free fatty acids in both MD simulations and NMR measurements [78]. In older studies, a similar shape of the S_{CD} profile was observed for highly asymmetric phosphatidylcholines [79]. In this work, we found that apart from the GM1 acyl chain, the interdigitation does not cause notable changes to the properties of other lipid chains, such as the sphingosine chain of GM1 or the acyl chains of POPC.

Atomistic simulations also revealed that the physical lipid bilayer properties such as average area per lipid and membrane thickness were not affected to any significant degree by changes in acyl chain length of GM1. Further, we found that the length of the acyl chain did not influence the conformation behavior and the orientation of the GM1 head group. These results (Figure S1, Figure S4, Table S2) are presented in Supplementary Information.

Long-chain GM1 perturbs the phase behavior of the opposing leaflet

The above atomistic results suggest that the interdigitation of long-chain GM1 such as $GM1_{30}$ reaches a level that can alter the order and thereby also the physical phase of the opposing leaflet. Large-scale simulations of the CG models were performed to test this assumption. Figure 6 shows structures for asymmetric many-component GM1:PSM:DLiPC:Chol membranes, where GM1 gangliosides with an extended acyl tail ($GM1_{extended}$) in the upper leaflet interdigitate to the lower monolayer. The membrane system in question undergoes spontaneous phase separation into L_o and L_d phases in the absence as well as in the presence of GM1. GM1 partitions to the L_o-phase, as expected, and it does not alter the in-plane phase behavior of the leaflet that hosts GM1 (Figure 6). However, the simulation structures (Figure 6) suggest that the long $GM1_{extended}$ chains perturb the structure of the opposite leaflet. More importantly, the data also propose that the transbilayer domain registry is altered by $GM1_{extended}$. To explore this idea, we first monitored the phase separation of the GM1-free leaflet in time. Figure 7 depicts for the GM1-free membrane that the contact fraction f_{mix} decreases to a significant degree in the course of time, indicating considerable phase separation. The systems with $GM1_{short}$ result in largely the same view. However, with long-chain $GM1_{extended}$ the situation changes. The long-chain GM1 perturbs the opposite leaflet to an extent that also influences its phase behavior: the phase separation process is slowed down, and the extent of phase separation is weakened compared to systems with $GM1_{short}$ or without any GM1. However, the diffusion coefficients of lipids in the opposite leaflet remain unaffected by the GM1 acyl chain length (Figure S5) and consequently the observed slowing down of phase separation does not result from reduced

mobility of lipids.

The rate of phase separation was quantified by fitting the time course of the contact fractions with an exponentially decaying function (see Methods). The average value of the decay constants (determined from the ten replicas for each system) was found to be 0.7 and 0.8 μs with 1.5 and 6 mol% of $GM1_{short,}$ respectively. With long-chain GM1, the average decay constant was observed to be 0.7 μs with 1.5 mol% and 0.9 μs with 6 mol% of $GM1_{extended}$. For comparison, in the GM1-free control system the decay constant to describe the rate of phase separation was 0.9 μs. These data suggest phase separation in a leaflet opposite to the $GM1_{short}$-rich monolayer to take place somewhat faster than phase separation opposite to a $GM1_{extended}$ –rich leaflet.

Similar conclusions can be drawn from Figure 8. It shows how 6 mol% of $GM1_{extended}$ slows down membrane registration significantly. More importantly, Figure 8 highlights that in the system with 6 mol% of this long-chain GM1 ($GM1_{extended}$), the interdigitating GM1 chains have a clear effect on the opposing leaflet, and disturbing its phase behavior (see Fig. 7) leads to the weakest domain registration between the two leaflets among the systems we studied.

Discussion

Glycosphingolipids constitute a diverse class of molecules both in terms of their glycan structure and fatty acids. Most frequently, fatty acids in GSLs are C16, C18, C20, C22, C24, and C24:1 [80], though shorter [81] C12 and C14 and longer [82, 83] C26-C36 fatty acids occur. Experimental evidence suggests that the chain length can affect ligand properties of the glycan headgroup. For instance, it was shown that long-chain GSLs enhance the binding of verotoxin [81]. Galectin-4, involved in apical transport, has been observed to have a strong preference for long-chain sulfatide (C24) [52]. In our study, we have selected GM1, known for its counterreceptor status for bacterial and tissue lectins. Earlier monolayer studies suggested that GSLs' acyl chain structure would affect the glycan's presentation, such that increasing exposure of GSL carbohydrates to the solvent would correlate positively with increasing acyl chain length [51]. However, our simulation results reported in this paper show hardly any impact of acyl chain length (ranging from 16 to 30 carbon atoms) on solvent accessibility or the conformation of the carbohydrate headgroup of GM1.

We found that a long acyl chain exhibits a very strong tendency to interdigitate, i.e., to protrude deep into the opposing bilayer. A deeper penetration of these chains into the opposing bilayer leaflet was observed to correlate with a substantial increase in the ordering at the chain end. The stronger the interdigitation, the more ordered the chain ends were observed to become. The observed interdigitation that takes place in a chain-length-dependent manner establishes a coupling between the two bilayer leaflets, as lipids in one leaflet can affect the structural properties of the other. Such behavior can be general for sphingolipids that are typically characterized by an inherent length asymmetry between their two chains [84].

The presented atomistic simulation data suggest that long-chain GM1 in the extracellular leaflet could modulate the phase behavior in the opposing cytosolic leaflet through GM1-induced membrane coupling. To explore this possibility, we used coarse-grained Martini simulations that allow considerations of sufficiently long times and large system sizes. In the simulations, GM1 resides exclusively in the extracellular leaflet, fully in line with experimental data. Our results showed spontaneous phase separation in GM1-containing membranes, where GM1 preferentially segregated into L_o domains. Given that the GM1 concentration in the simulations was low, the observed separation is in line with earlier Martini simulation studies [85]. Furthermore, based on experiments, phase separation takes place in mixtures of PSM and cholesterol together with dioleoylphosphatidylcholine [86]. In the present simulations for GM1 with a shorter acyl chain (~18 carbons), the two bilayer leaflets exhibited perfect registry, *i.e.,* they were phase-symmetric. In contrast, GM1 with an extended acyl chain (~30 carbons) was observed to perturb the phase behavior of the GM1-free cytosolic leaflet. A long GM1 acyl chain that interdigitated into the opposite leaflet induced mixing between saturated and unsaturated lipids, thereby preventing or at least slowing down the ideal phase separation in the cytosolic leaflet. This result is consistent with an earlier experimental study, which showed the existence of an intermediate phase in the region opposite to an L_o domain [23].

In aggregate, the present study shows a connection between GM1 acyl chain length and bilayer phase behavior. Interleaflet coupling is strongly promoted by long-chain GM1-induced interdigitation, which modulates the phase behavior in the opposing membrane leaflet. Such a physical interaction between the leaflets offers a plausible mechanism for mediating or fostering signaling across asymmetric membranes.

Acknowledgements

Reinis Danne is thanked for technical support at the early stage of this work. CSC – IT Center for Science (Espoo, Finland) is acknowledged for computer resources. European Research Council (Advanced Grant project CROWDED-PRO-LIPIDS) and the Academy of Finland (Centre of Excellence program) are thanked for financial support.

Supplementary Information

Additional results and discussion.

References

[1] G. van Meer, D. R. Voelker, G. W. Feigenson, Membrane lipids: Where they are and how they behave, Nature Rev. Mol. Cell Biol. 9 (2008) 112–124.

[2] M. Ikeda, A. Kihara, Y. Igarashi, Lipid asymmetry of the eukaryotic plasma membrane: Functions and related enzymes, Biol. Pharmaceut. Bull. 29 (2006) 1542–1546.

[3] J. Kopitz, Glycolipids, in: H. J. Gabius (Ed.) The Sugar Code. Fundamentals of glycosciences, Wiley-VCH, Weinheim, Germany, 2009, pp. 177–198.

[4] C. L. Schengrund, Gangliosides: Glycosphingolipids essential for normal neural development and function, Trends Biochem. Sci. 40 (2015) 397–406.

[5] H. J. Gabius, J. C. Manning, J. Kopitz, S. André, H. Kaltner, Sweet complementarity: The functional pairing of glycans with lectins, Cell Mol. Life Sci. 73 (2016) 1989–2016.

[6] H. J. Gabius, H. Kaltner, J. Kopitz, S. André, The glycobiology of the CD system: A dictionary for translating marker designations into glycan/lectin structure and function, Trends Biochem. Sci. 40 (2015) 360–376.

[7] T. Róg, I. Vattulainen, Cholesterol, sphingolipids, and glycolipids: What do we know about their role in raft-like membranes, Chem. Phys. Lipids 184 (2014) 82–104.

[8] M. C. Rheinstädter, O. G. Mouritsen, Small-scale structure in fluid cholesterol-lipid bilayers. Curr. Opin. Colloid Interface Sci. 18 (2013) 440–447.

[9] P. F. F. Almeida, Thermodynamics of lipid interactions in complex bilayers, Biochim. Biophys. Acta 1788 (2009) 72–85.

[10] L. J. Pike, Rafts defined: A report on the Keystone Symposium on Lipid Rafts and Cell Function, J. Lipid Res. 47 (2006) 1597–1598.

[11] K. Simons, E. Ikonen, Functional rafts in cell membranes, Nature 387 (1997) 569–572.

[12] D. Lingwood, K. Simons, Lipid rafts as an organizing principle, Science 327 (2010) 46–50.

[13] E. Sevcsik, G. J. Schuetz, With or without rafts? Alternative views on cell membranes,

Bioessays 38 (2016) 129–139.

[14] F. X. Contreras, A. M. Ernst, F. Wieland, B. Brügger, Specificity of intramembrane protein-lipid interactions, Cold Spring Harb. Perspect. Biol. 3 (2011) a004705.

[15] L. A. Bagatolli, O. G. Mouritsen, Is the fluid mosaic (and the accompanying raft hypothesis) a suitable model to describe fundamental features of biological membranes? What may be missing? Front. Plant Sci. 4 (2013) 457.

[16] D. A. Brown, E. London, Structure and origin of ordered lipid domains in biological membranes, J. Membr. Biol. 164 (1998) 103–114.

[17] H. J. Risselada, S. J. Marrink, The molecular face of lipid rafts in model membranes, Proc. Natl. Acad. Sci. U. S. A. 105 (2008) 17367–17372.

[18] V. Kiessling, J. M. Crane, L. K. Tamm, Transbilayer effects of raft-like lipid domains in asymmetric planar bilayers measured by single molecule tracking, Biophys. J. 91 (2006) 3313–3326.

[19] T.-Y. Wang, J. R. Silvius, Cholesterol does not induce segregation of liquid-ordered domains in bilayers modeling the inner leaflet of the plasma membrane, Biophys. J. 81 (2001) 2762–2773.

[20] S. May, Trans-monolayer coupling of fluid domains in lipid bilayers, Soft Matter 5 (2009) 3148–3156.

[21] J. D. Nickels, X. Cheng, B. Mostofian, C. Stanley, B. Lindner, F. A. Heberle, S. Perticaroli, M. Feygenson, T. Egami, R. F. Standaert, J. C. Smith, D. A. A. Myles, M. Ohl, J. Katsaras, J. Am. Chem. Soc. 137 (2015) 15772–15780.

[22] L. Tayebi, Y. Ma, D. Vashaee, G. Chen, S. K. Sinha, A. N. Parikh, Long-range interlayer alignment of intralayer domains in stacked lipid bilayers, Nature Materials 11 (2012) 1074–1080.

[23] M. D. Collins, S. L. Keller, Tuning lipid mixtures to induce or suppress domain formation across leaflets of unsupported asymmetric bilayers, Proc. Natl. Acad. Sci. U.S.A. 105 (2008) 124–128.

[24] W. C. Lin, C. D. Blanchette, T. V. Ratto, M. L. Longo, Lipid asymmetry in DLPC/DSPC- supported lipid bilayers: A combined AFM and fluorescence microscopy study, Biophys. J. 90 (2006) 228–237.

[25] S. Leibler, D. Andelman, Ordered and curved meso-structures in membranes and amphiphilic films, J. de Physique 48 (1987) 2013–2018.

[26] J. D. Perlmutter, J. N. Sachs, Interleaflet interaction and asymmetry in phase separated lipid bilayers: Molecular dynamics simulations, J. Am. Chem. Soc. 133 (2011) 6563–6577.

[27] T. Rog, A. Orlowski, A. Llorente, T. Skotland, T. Sylvanne, D. Kauhanen, K. Ekroos, K. Sandvig, I. Vattulainen, Interdigitation of long-chain sphingomyelin induces coupling of membrane leaflets in a cholesterol dependent manner, Biochim. Biophys. Acta 1858 (2016) 281–288.

[28] A. P. Ramos, P. Lagüe, G. Lamoureux, M. Lafleur, Effect of saturated very long-chain fatty acids on the organization of lipid membranes: A study combining 2H NMR spectroscopy and molecular dynamics simulations, J. Phys. Chem. B 120 (2016) 6951–6960.

[29] C. Wan, V. Kiessling, L. K. Tamm, Coupling of cholesterol-rich lipid phases in asymmetric bilayers, Biochemistry 47 (2008) 2190–2198.

[30] D. A. Pantano, P. B. Moore, M. L. Klein, D. E. Discher, Raft registration across bilayers in a molecularly detailed model, Soft Matter 7, (2011) 8182–8191.

[31] J. J. Williamson, P. D. Olmsted, Registered and antiregistered phase separation of mixed amphiphilic bilayers, Biophys. J. 108 (2015) 1963–1976.

[32] J. J. Williamson, P. D. Olmsted, Nucleation of symmetric domains in the coupled leaflets of a bilayer, Soft Matter 11 (2015) 8948–8959.

[33] T. Han, T. P. Bailey, M. Haataja, Hydrodynamic interaction between overlapping domains during recurrence of registration within planar lipid bilayer membranes, Phys. Rev. E 89 (2014) 032717.

[34] H. J. Gabius (Ed.) The Sugar Code. Fundamentals of Glycosciences, in: Wiley-VCH, Weinheim, Germany, 2009.

[35] H. J. Gabius, S. André, J. Jiménez-Barbero, A. Romero, D. Solís, From lectin structure to functional glycomics: Principles of the sugar code, Trends Biochem. Sci. 36 (2011) 298–313.

[36] H. J. Gabius, The magic of the sugar code, Trends Biochem. Sci. 40 (2015) 341.

[37] M. Manna, T. Rog, I. Vattulainen, The challenges of understanding glycolipid functions: An open outlook based on molecular simulations, Biochim. Biophys. Acta – Mol. Cell Biol. Lipids 1841 (2014) 1130–1145.

[38] A. Hall, T. Rog, I. Vattulainen, Effect of galactosylceramide on the dynamics of cholesterol-rich lipid membranes, J. Phys. Chem. B 115 (2011) 14424–14434.

[39] D. Lingwood, B. Binnington, T. Rog, I. Vattulainen, M. Grzybek, U. Coskun, C. A. Lingwood, K. Simons, Cholesterol modulates glycolipid conformation and receptor activity, Nature Chem. Biol. 7 (2011) 260–262.

[40] M. Manna, C. Mukhopadhyay, Binding, conformational transition and dimerization of amyloid-beta peptide on GM1-containing ternary membrane: Insights from molecular dynamics simulation, PLoS One 8 (2013) e71308.

[41] R. W. Ledeen, G. Wu, The multi-tasked life of GM1 ganglioside, a true factotum of nature, Trends Biochem. Sci. 40 (2015) 407-418.

[42] J. Kopitz, C. von Reitzenstein, M. Burchert, M. Cantz, H. J. Gabius, Galectin-1 is a major receptor for ganglioside GM1, a product of the growth-controlling activity of a cell surface ganglioside sialidase, on human neuroblastoma cells in culture, J. Biol. Chem. 273 (1998) 11205-11211.

[43] J. Kopitz, C. von Reitzenstein, S. André, H. Kaltner, J. Uhl, V. Ehemann, M. Cantz, H. J. Gabius, Negative regulation of neuroblastoma cell growth by carbohydrate-dependent surface binding of galectin-1 and functional divergence from galectin-3, J. Biol. Chem. 276 (2001) 35917-35923.

[44] R. Fajka-Boja, A. Blasko, F. Kovacs-Solyom, G.J. Szebeni, G.K. Toth, E. Monostori, Co-localization of galectin-1 with GM1 ganglioside in the course of its clathrin- and raft-dependent endocytosis, Cell. Mol. Life Sci. 65 (2008) 2586-2593.

[45] J. Wang, Z. H. Lu, H. J. Gabius, C. Rohowsky-Kochan, R.W. Ledeen, G. Wu, Cross-linking of GM1 ganglioside by galectin-1 mediates regulatory T cell activity involving TRPC5 channel activation: possible role in suppressing experimental autoimmune encephalomyelitis, J. Immunol. 182 (2009) 4036-4045.

[46] G. Wu, Z. H. Lu, S. Andre, H. J. Gabius, R. W. Ledeen, Functional interplay between ganglioside GM1 and cross-linking galectin-1 induces axon-like neuritogenesis via integrin-based signaling and TRPC5-dependent Ca(2+) influx, J. Neurochem. 136 (2016) 550–563.

[47] R. W. Ledeen, G. Wu, S. André, D. Bleich, G. Huet, H. Kaltner, J. Kopitz, H. J. Gabius, Beyond glycoproteins as galectin counterreceptors: Tumor/effector T cell growth control via ganglioside GM1, Ann. N. Y. Acad. Sci. 1253 (2012) 206–221.

[48] J. Kopitz, M. Bergmann, H. J. Gabius, How adhesion/growth-regulatory galectins-1 and -3 attain cell specificity: Case study defining their target on neuroblastoma cells (SK-N-MC) and marked affinity regulation by affecting microdomain organization of the membrane, IUBMB Life 62 (2010) 624–628.

[49] J. Majewski, S. André, E. Jones, E. Chi, H. J. Gabius, X-ray reflectivity and grazing incidence diffraction studies of interaction between huma adhesion/growth-regulatory galectin-1 and DPPE:GM1 lipid monolayer at the air/water interface, Biochemistry (Moscow) 80 (2015) 943–956.

[50] K. Iwabuchi, H. Nakayama, C. Iwahara, K. Takamori, Significance of glycosphingolipid fatty acid chain length on membrane microdomain-mediated signal transduction, FEBS Lett. 584 (2010) 1642–1652.

[51] E. B. Watkins, H. Gao, A. J. C. Dennison, N. Chopin, B. Struth, T. Arnold, J.-C. Florent, L. Johannes, Carbohydrate conformation and lipid condensation in mono layers containing glycosphingolipid Gb3: Influence of acyl chain structure, Biophys. J. 107 (2014) 1146–1155.

[52] D. Delacour, V. Gouyer, J. P. Zanetta, H. Drobecq, E. Leteurtre, G. Grard, O. Moreau-Hannedouche, E. Maes, A. Pons, S. Andre, A. Le Bivic, H. J. Gabius, A. Manninen, K. Simons, G. Huet, Galectin-4 and sulfatides in apical membrane trafficking in enterocyte-like cells, J. Cell Biol. 169 (2005) 491–501.

[53] L. Stechly, W. Morelle, A. F. Dessein, S. André, G. Grard, D. Trinel, M. J. Dejonghe, E. Leteurtre, H. Drobecq, G. Trugnan, H. J. Gabius, G. Huet, Galectin-4-regulated delivery of glycoproteins to the brush border membrane of enterocyte-like cells, Traffic 10 (2009) 438–450.

[54] S. Velasco, N. Díez-Revuelta, T. Hernández-Iglesias, H. Kaltner, S. André, H. J. Gabius, J. Abad-Rodríguez, Neuronal galectin-4 is required for axon growth and for the organization of axonal membrane L1 delivery and clustering, J. Neurochem. 125 (2013) 49–62.

[55] R. F. M. de Almeida, L. M. S. Loura, A. Fedorov, M. Prieto, Lipid rafts have different sizes depending on membrane composition: A time-resolved fluorescence resonance energy transfer study, J. Mol. Biol. 346 (2005) 1109–1120.

[56] W. L. Jorgensen, D. S. Maxwell, J. TiradoRives, Development and testing of the OPLS all-atom force field on conformational energetics and properties of organic liquids, J. Am. Chem. Soc. 118 (1996) 11225–11236.

[57] W. Damm, A. Frontera, J. TiradoRives, W. L. Jorgensen, OPLS all-atom force field for carbohydrates, J. Comput. Chem. 18 (1997) 1955–1970.

[58] W. Kulig, M. Pasenkiewicz-Gierula, T. Róg, Cis and trans unsaturated phosphatidylcholine bilayers: A molecular dynamics simulation study, Chem. Phys. Lipids 195 (2016) 12–20.

[59] W. Kulig, M., Pasenkiewicz-Gierula, T. Rog, Topologies, structures and parameter files for lipid simulations in GROMACS with the OPLS-AA force field: DPPC, POPC, DOPC, PEPC, and cholesterol, Data in Brief 5 (2015) 333–336.

[60] A. Maciejewski, M. Pasenkiewicz-Gierula, O. Cramariuc, I. Vattulainen, T. Rog, Refined OPLS all-atom force field for saturated phosphatidylcholine bilayers at full hydration, J. Phys. Chem. B 118 (2014) 4571–4581.

[61] T. Róg, A. Orłowski, A. Llorente, T. Skotland, T. Sylvänne, D. Kauhanen, K. Ekroos, K. Sandvig, I. Vattulainen, Package of GROMACS input files for molecular dynamics simulations of mixed, asymmetric bilayers including molecular topologies, equilibrated structures, and force field for lipids compatible with OPLS-AA parameters, Data in Brief 7 (2016) 1171–1174.

[62] W. L. Jorgensen, J. Chandrasekhar, J. D. Madura, R. W. Impey, M. L. Klein, Comparison of simple potential functions for simulating liquid water, J. Chem. Phys. 79 (1983) 926–935.

[63] B. Hess, C. Kutzner, D. van der Spoel, E. Lindahl, GROMACS 4: Algorithms for highly efficient, load-balanced, and scalable molecular simulation, J. Chem. Theory Comput. 4 (2008) 435–447.

[64] G. Bussi, D. Donadio, M. Parrinello, Canonical sampling through velocity rescaling, J. Chem. Phys. 126 (2007) 014101.

[65] M. Parrinello, A. Rahman, Polymorphic transitions in single crystals: A new molecular dynamics method, J. Appl. Phys. 52 (1981) 7182–7190.

[66] T. Darden, D. York, L. Pedersen, Particle mesh Ewald: An N log(N) method for Ewald sums in large systems, J. Chem. Phys. 98 (1993) 10089–10092.

[67] B. Hess, H. Bekker, H. J. C. Berendsen, J. Fraaije, LINCS: A linear constraint solver for

molecular simulations, J. Comput. Chem. 18 (1997) 1463–1472.

[68] S. J. Marrink, H. J. Risselada, S. Yefimov, D. P. Tieleman, A. H. de Vries, The Martini force field: Coarse grained model for biomolecular simulations, J. Phys. Chem. B 111 (2007) 7812–7824.

[69] C. A. Lopez, Z. Sovova, F. J. van Eerden, A. H. de Vries, S. J. Marrink, Martini force field parameters for glycolipids, J. Chem. Theory Comput. 9 (2013) 1694–1708.

[70] M. N. Melo, H. I. Ingolfsson, S. J. Marrink, Parameters for Martini sterols and hopanoids based on a virtual-site description, J. Chem. Phys. 143 (2015) 243152.

[71] H. J. Risselada, S. J. Marrink, The molecular face of lipid rafts in model membranes, Proc. Natl. Acad. Sci. USA 105 (2008) 17367–17372.

[72] L. V. Schäfer and S. J. Marrink, Partitioning of lipids at domain boundaries in model membranes, Biophys. J. 99 (2010) L91-L93.

[73] M. J. Abraham, T. Murtola, R. Schulz, S. Páll, J. C. Smith, B. Hess, E. Lindahl GROMACS: High performance molecular simulations through multi-level parallelism from laptops to supercomputers, Software X 1-2 (2015) 19–25.

[74] J. H. Davis, The description of membrane lipid conformation, order and dynamics by 2H-NMR, Biochim. Biophys. Acta 737 (1983) 117–171.

[75] H. C. Siebert, S. André, S. Y. Lu, M. Frank, H. Kaltner, J. A. van Kuik, E. Y. Korchagina, N. V. Bovin, E. Tajkhorshid, R. Kaptein, J. F. G. Vliegenthart, C. W. von der Lieth, J. Jiménez-Barbero, J. Kopitz, H. J. Gabius, Unique conformer selection of human growth-regulatory lectin galectin-1 for ganglioside GM1 versus bacterial toxins, Biochemistry 42 (2003) 14762–14773.

[76] C. Das, M. G. Noroand, P. D. Olmsted, Simulation studies of stratum corneum lipid mixtures, Biophys. J. 97 (2009) 1941–1951.

[77] J. Domanski, S. J. Marrink, L. V. Schafer, Transmembrane helices can induce domain formation in crowded model membranes, Biochim. Biophys. Acta 1818 (2012) 984–994.

[78] A. P. Ramos, P. Lagüe, G. Lamoureux, M. Lafleur, Effect of saturated very long-chain fatty acids on the organization of lipid membranes: A study combining 2H NMR spectroscopy and molecular dynamics simulations, J. Phys. Chem. B 120 (2016) 6951–6960.

[79] R. N. Lewis, R. N. McElhaney, M. A. Monck, P. R. Cullis, Studies of highly asymmetric mixed-chain diacyl phosphatidylcholines that form mixed-interdigitated gel phases: Fourier transform infrared and 2H NMR spectroscopic studies of hydrocarbon chain conformation and orientational order in the liquid-crystalline state, Biophys. J. 67 (1994) 197–207.

[80] A. Pellizzari, H. Pang, C. A. Lingwood, Binding of verocytotoxin 1 to its receptor is influenced by differences in receptor fatty acid content, Biochemistry 31 (1992) 1363–1370.

[81] A. Kiarash, B. Boyd, C. A. Lingwood, Glycosphingolipid receptor function is modified by fatty acid content. Verotoxin 1 and verotoxin 2c preferentially recognize different

globotriaosyl ceramide fatty acid homologues, J. Biol. Chem. 269 (1994) 11138–11146.

[82] R. Sandhoff, Very long chain sphingolipids: Tissue expression, function and synthesis, FEBS Lett. 584 (2010) 1907–1913.

[83] D. Solís, N. V. Bovin, A. P. Davis, J. Jiménez-Barbero, A. Romero, R. Roy, K. Smetana Jr., H-J. Gabius, A guide into glycosciences: How chemistry, biochemistry and biology cooperate to crack the sugar code, Biochim. Biophys. Acta 1850 (2015) 186–235.

[84] I. E. Mehlhorn, E. Florio, K. R. Barber, C. Lordo, C. W. M. Grant, Evidence that trans-bilayer interdigitation of glycosphingolipid long chain fatty acids may be a general phenomenon, Biochim. Biophys. Acta 939 (1988) 151–159.

[85] S. Baoukina, E. Mendez-Villuendas, W. F. D. Bennett, D. P. Tieleman, Computer simulations of the phase separation in model membranes, Faraday Disc. 161 (2013) 63–75.

[86] D. Marsh, CRC Handbook of Lipid Bilayers (CRC Press, Boca Raton, 1990).

Table 1. Compositions of the atomistic and coarse-grained lipid bilayer models.

Bilayer	**Lipid composition**	**GM1 type (number of carbon atoms or beads in the acyl chain)**	**Simulation length**
Symmetric bilayers (all-atom model)	GM1:Chol:POPC = 4.86:25:70.14	$GM1_{16}$ (16 carbon atoms) or $GM1_{18}$ (18 carbon atoms) or … or $GM1_{30}$ (30 carbon atoms)	400 ns each (16 bilayers) = 6.4 μs
	GM1:POPC = 6.48:93.52		
Asymmetric bilayers (coarse-grained model)	GM1:PSM:DLiPC:Chol = 1.50:28.5:40:30 [GM1-rich leaflet] GM1:PSM:DLiPC:Chol = 0:30:40:30 [GM1-free leaflet]	$GM1_{short}$ (5 beads, corresponds to ~18 carbon atoms) or $GM1_{extended}$ (8 beads, corresponds to ~30 carbon atoms)	For 1.5 mol%, 10 μs each (3 bilayers) x 10 repeats each = 300 μs; for 6 mol% $GM1_{extended}$, 20 μs x 20 repeats = 200 μs.
	GM1:PSM:DLiPC:Chol = 6:27:38.5:28.5 [GM1-rich leaflet] GM1:PSM:DLiPC:Chol = 0:30:40:30 [GM1-free leaflet]		
Symmetric bilayer (coarse-grained model)	GM1:PSM:DLiPC:Chol = 0:30:40:30	GM1-free model (control system)	10 μs x 8 repeats = 80 μs

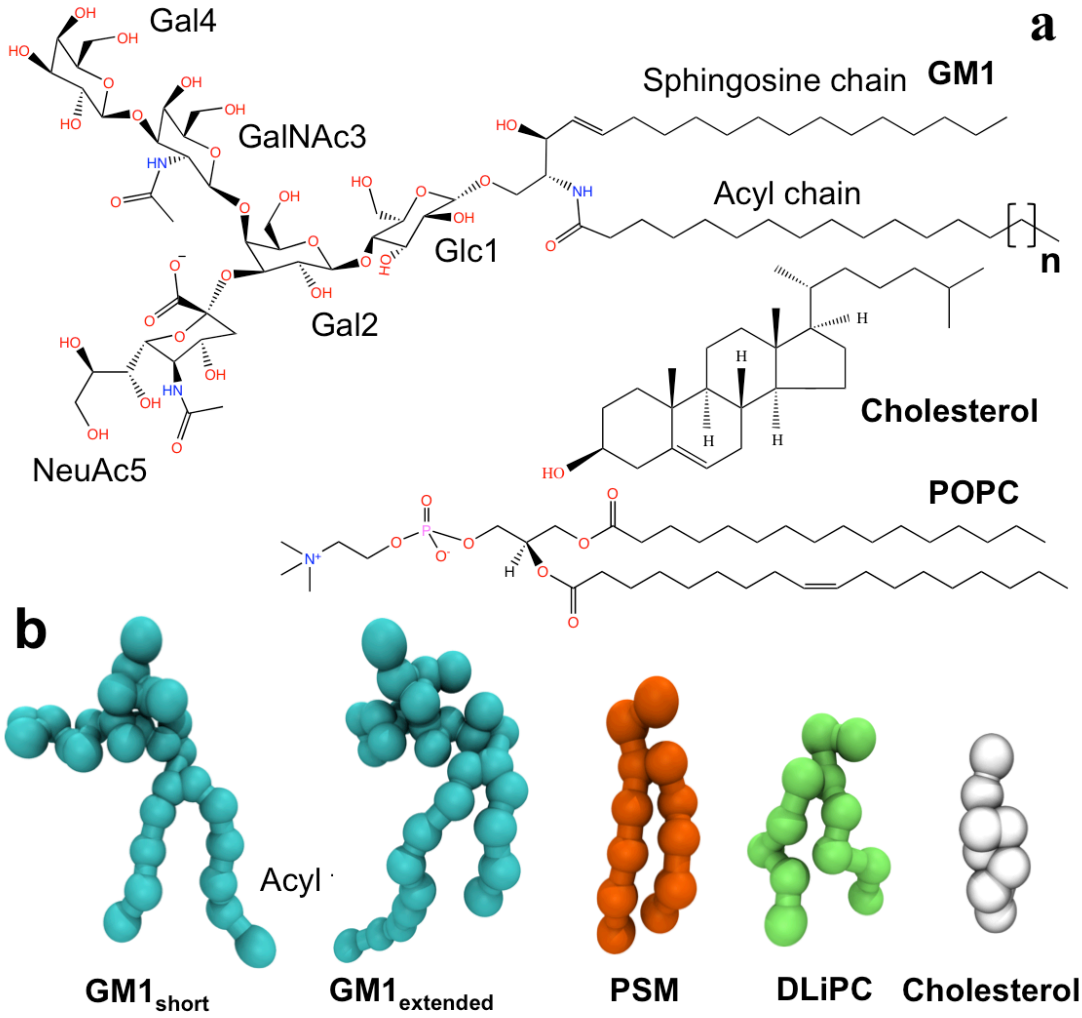

Figure 1. Chemical structure different lipid species used for (a) all-atom and (b) coarse-grained simulations. In atomistic simulations, the acyl chain length of GM1 was varied from 16 to 30 carbon atoms. In coarse-grained simulations, GM1 had an acyl chain with either five ($GM1_{short}$) or eight beads ($GM1_{extended}$).

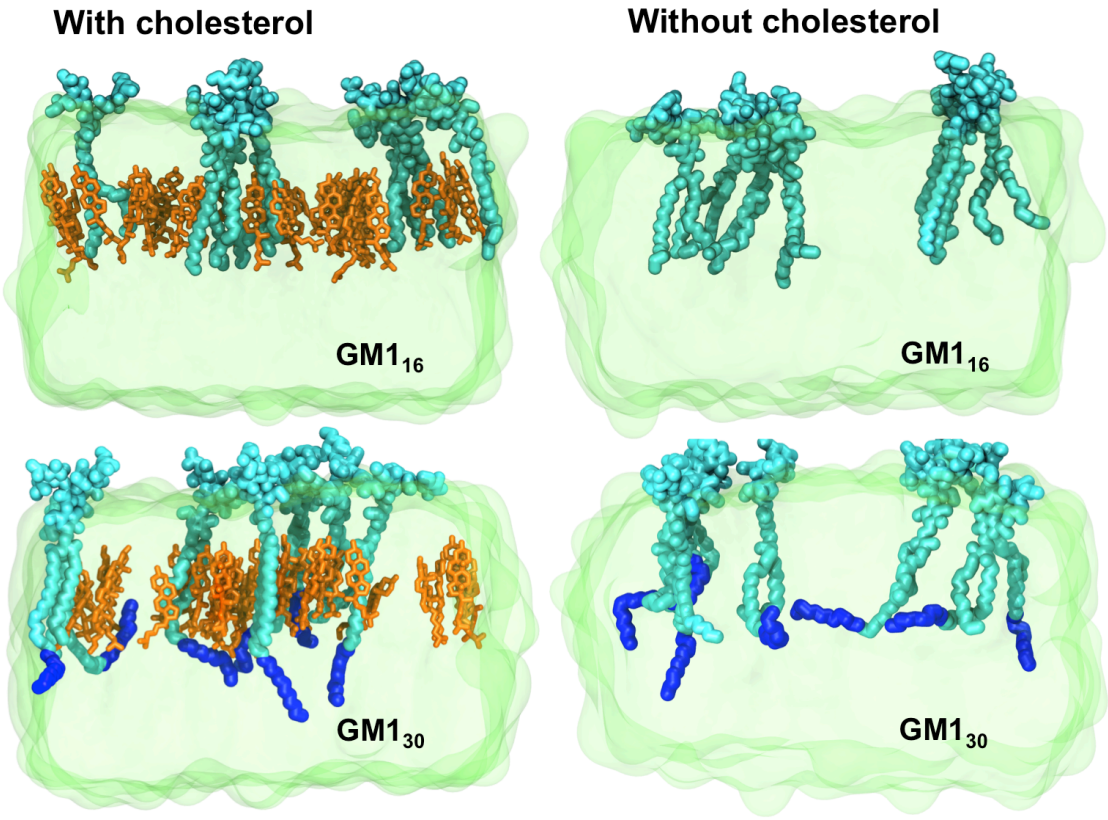

Figure 2. Snapshots of symmetric bilayers with the shortest ($GM1_{16}$, upper panel) and the longest ($GM1_{30}$, lower panel) ganglioside in the atomistic simulations. For clarity, bilayers are shown as a green transparent surface, where dark green depicts the edges of the bilayer region. GM1 (cyan) and cholesterol (orange) molecules are shown only in the upper leaflet, and POPC is not shown. For $GM1_{30}$, carbon atoms beyond the 18^{th} carbon are shown in blue.

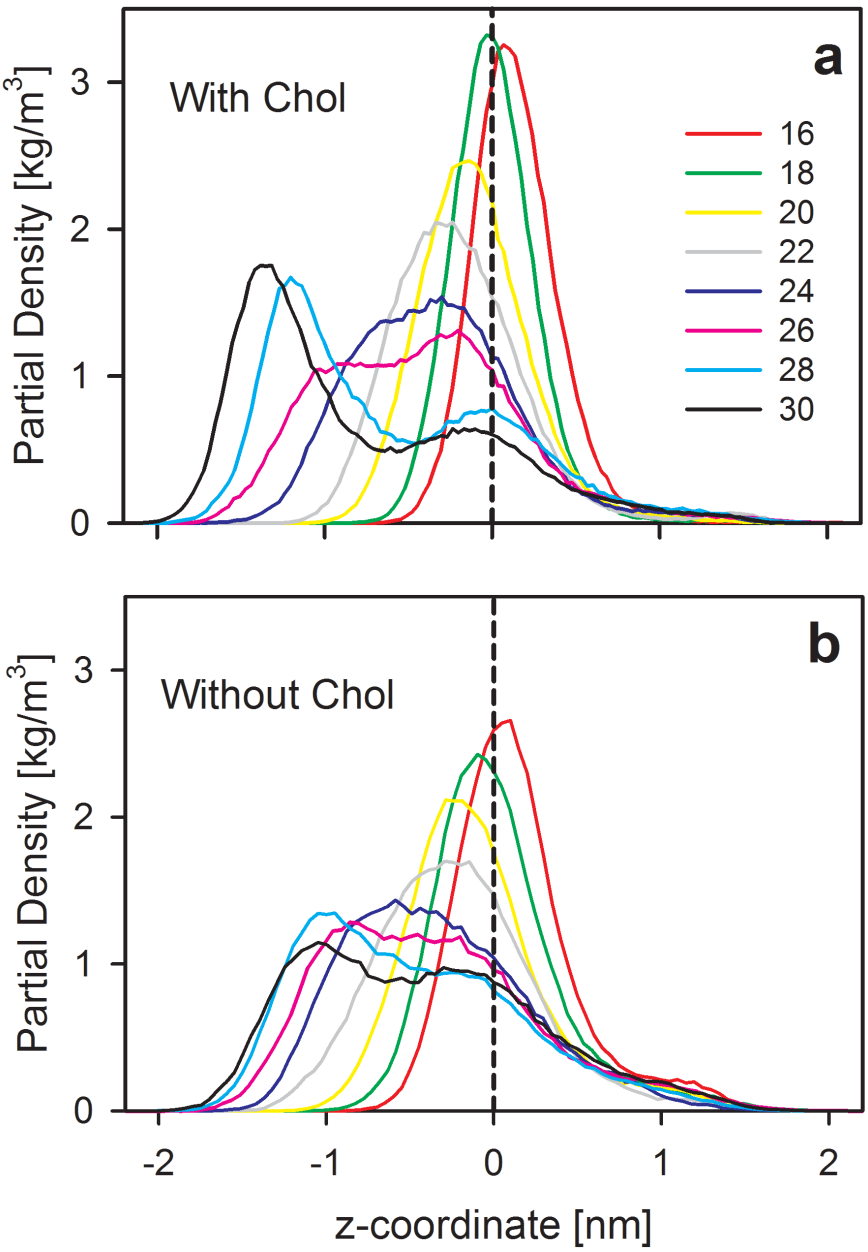

Figure 3. Partial density profiles (atomistic simulations) showing the distribution of the terminal carbon atom of the GM1 acyl chain in membranes (a) with cholesterol (Chol) and (b) without it, with varying length of the GM1 acyl chain. GM1 molecules considered here locate in the upper leaflet with $z > 0$ and interdigitate to the lower leaflet with $z < 0$.

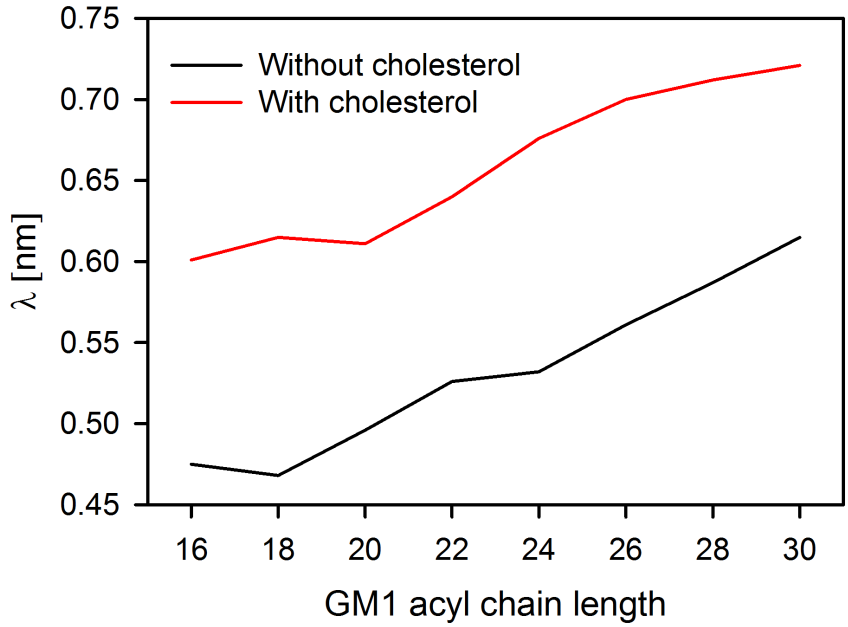

Figure 4. Values of λ (in units of nm) for systems (red) with and (black) without cholesterol as a function of GM1 acyl chain length (atomistic simulations).

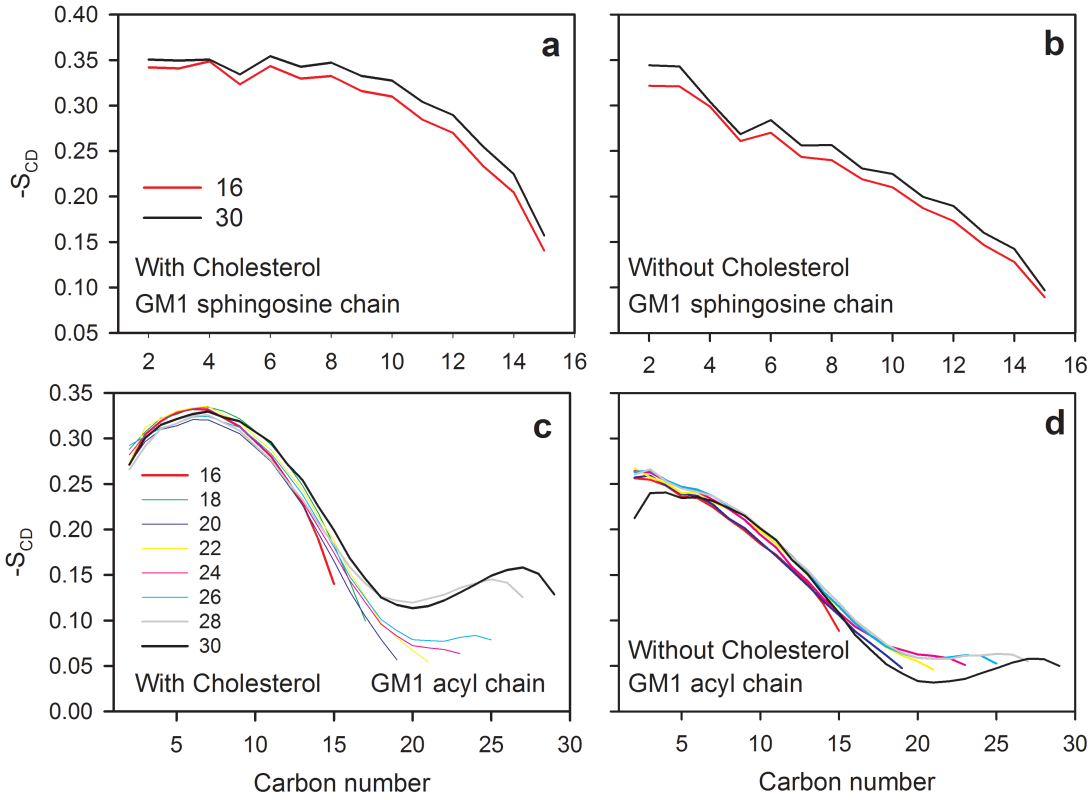

Figure 5. S_{CD} order parameter profiles of GM1 chains shown in terms of the carbon number in the chain: (a, b) sphingosine and (c, d) acyl chain, in membranes (a, c) with, and (b, d) without cholesterol.

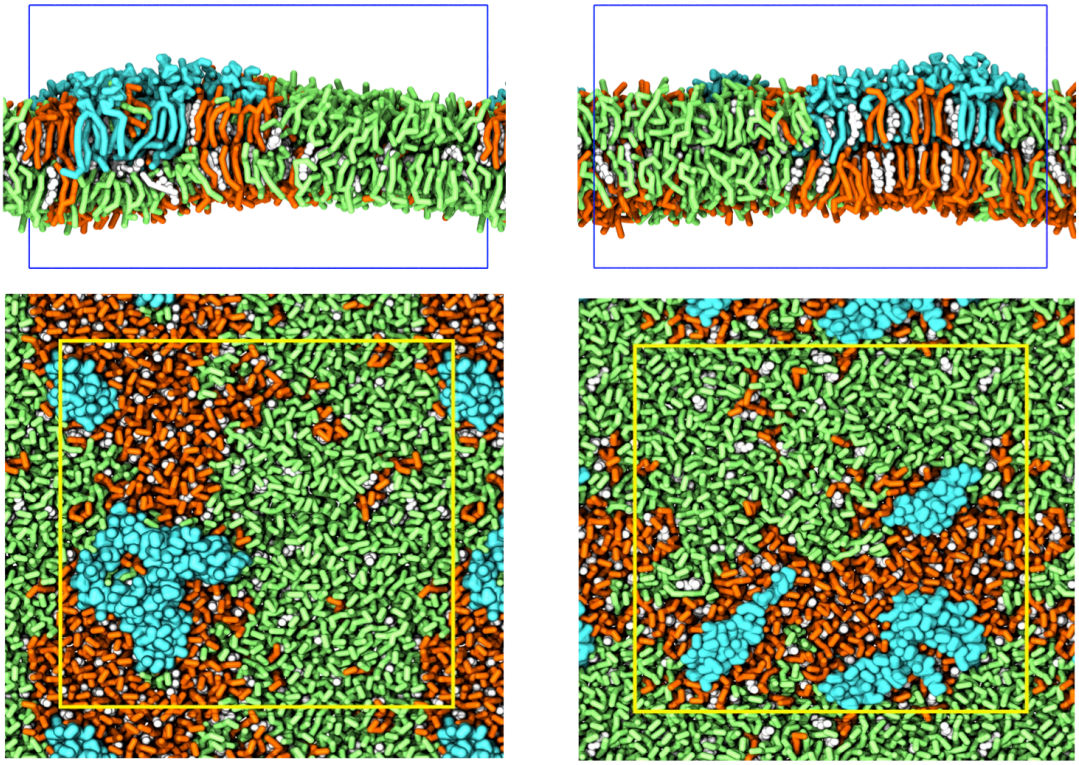

Figure 6. Final simulation structures of coarse-grained systems containing 6 mol% of (left) $GM1_{extended}$ or (right) $GM1_{short}$, viewed from (top row) the side and from (bottom row) above. PSM is pictured in orange, DLiPC in green, cholesterol in white, and GM1 in cyan. Water and ions have been omitted from the images for clarity.

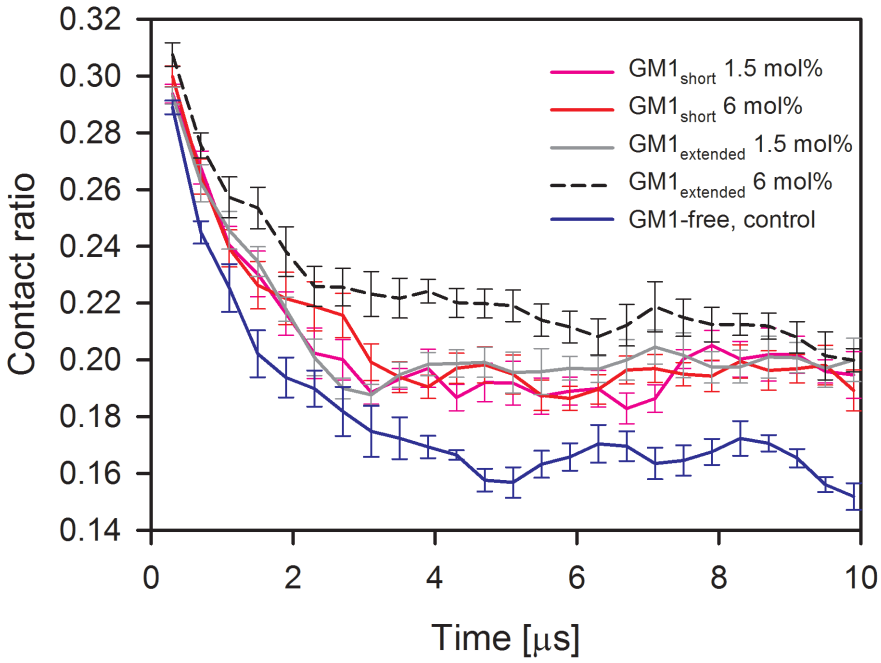

Figure 7. Contact ratio between PSM and DLiPC lipids during CG simulations that start from a random initial configuration and evolve towards phase separation.

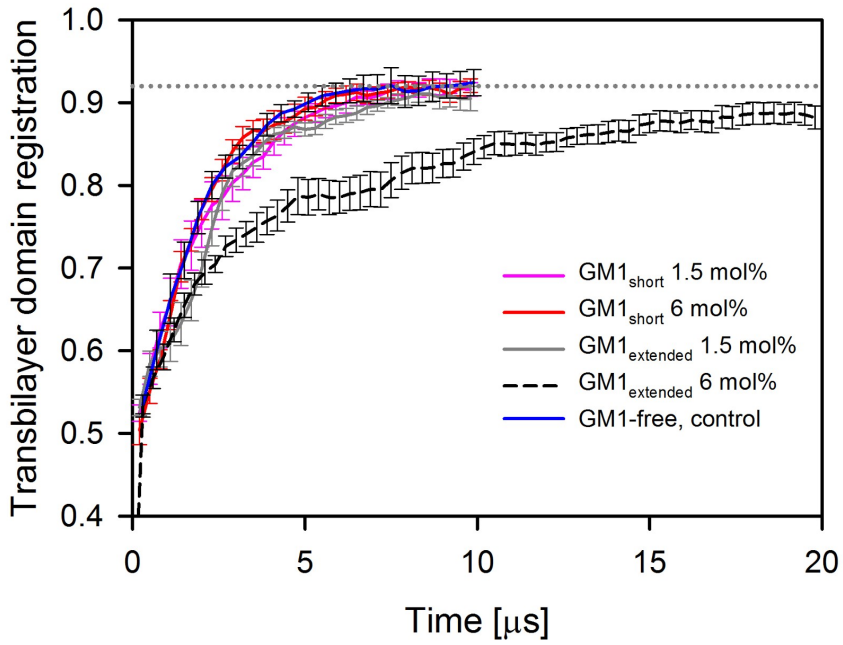

Figure 8. Transbilayer domain registration in the different systems (CG simulations). The gray dotted line highlights the value where the data of the simulated systems (except for $GM1_{extended}$ (6 mol%)) converge.

Table of Contents Graphic